Instantaneous normal mode analysis for intermolecular and intramolecular vibrations of water from atomic point of view

Yu-Chun Chen, Ping-Han Tang, and Ten-Ming Wu

Citation: The Journal of Chemical Physics **139**, 204505 (2013); doi: 10.1063/1.4829679
View online: http://dx.doi.org/10.1063/1.4829679
View Table of Contents: http://scitation.aip.org/content/aip/journal/jcp/139/20?ver=pdfcov
Published by the AIP Publishing

Instantaneous normal mode analysis for intermolecular and intramolecular vibrations of water from atomic point of view

Yu-Chun Chen,[1] Ping-Han Tang,[1] and Ten-Ming Wu[1,2,a)]
[1]*Institute of Physics, National Chiao-Tung University, Hsinchu 300, Taiwan*
[2]*National Center for Theoretical Sciences, Hsinchu 300, Taiwan*

(Received 16 July 2013; accepted 28 October 2013; published online 27 November 2013)

By exploiting the instantaneous normal mode (INM) analysis for models of flexible molecules, we investigate intermolecular and intramolecular vibrations of water from the atomic point of view. With two flexible SPC/E models, our investigations include three aspects about their INM spectra, which are separated into the unstable, intermolecular, bending, and stretching bands. First, the O- and H-atom contributions in the four INM bands are calculated and their stable INM spectra are compared with the power spectra of the atomic velocity autocorrelation functions. The unstable and intermolecular bands of the flexible models are also compared with those of the SPC/E model of rigid molecules. Second, we formulate the inverse participation ratio (IPR) of the INMs, respectively, for the O- and H-atom and molecule. With the IPRs, the numbers of the three species participated in the INMs are estimated so that the localization characters of the INMs in each band are studied. Further, by the ratio of the IPR of the H atom to that of the O atom, we explore the number of involved OH bond per molecule participated in the INMs. Third, by classifying simulated molecules into subensembles according to the geometry of their local environments or their H-bond configurations, we examine the local-structure effects on the bending and stretching INM bands. All of our results are verified to be insensible to the definition of H-bond. Our conclusions about the intermolecular and intramolecular vibrations in water are given. © *2013 AIP Publishing LLC*. [http://dx.doi.org/10.1063/1.4829679]

I. INTRODUCTION

Water is ubiquitous in nature and important to biological systems. Researches about water are actively in progress. The dynamic and structural information of water at ambient conditions can be obtained via its vibrational spectroscopy.[1] From collective vibrations among molecules to the stretching vibrations of OH bonds, the vibrational spectroscopy of water covers quite a broad range in frequency and has been measured by different kinds of experiments, including conventional IR absorption,[2–4] Raman scattering,[5–8] the OHD-RIKES method,[9] and recently developed ultrafast techniques,[10–13] such as the two-dimensional IR measurement[14–17] and the sum frequency generation.[18,19] Fluctuating in time and changing patterns frequently,[20] the H-bond network in water causes many unusual physical properties and makes its vibrational spectroscopy not fully understood so far.

The vibrational spectroscopy of water is affected by both molecular motions and local structures in the liquid phase.[12,21] Because of their local environments, individual molecules possess different vibrational frequencies, which result in the inhomogeneous broadening via an ensemble average over liquid configurations. This broadening carries no dynamic information. On the other hand, molecular motions, strongly influenced by intermolecular forces, produce dephasing in vibrational modes of molecules. In the dephasing time scale, molecular dynamics gives rise to the so-called homogeneous broadening in the line shape, for this effect is identical for all molecules.[21] In the past two decades, the ultrafast and conventional vibrational spectroscopy of water have been intensively studied by various theories.[22–31] Among them, by treating molecular motions with classical mechanics, the instantaneous normal mode (INM) theory is the one from the viewpoint of potential energy landscape.[32,33]

Nowadays, the INM theory has been developed as an analytical tool to study the vibrational modes in disordered systems and some results by this analysis have been reported recently.[34–40] In general, the density of states (DOS) of INMs can be related to the vibrational spectrum observed by experiments. On the other hand, with inverse participation ratio (IPR),[41] the localization of INMs can be studied. In such a way, the INM analysis is useful for exploring microscopically the vibrational spectroscopy.

For water, the INM spectra of several models have been reported.[42–46] For models of rigid molecules, the INM spectrum consists of the intermolecular and unstable branches, corresponding to the real and imaginary INM frequencies, respectively. From the molecular point of view, in which molecules in the gas phase are considered as the basic units, the INM spectrum of a rigid-molecule model is attributed to components associated with the translational and orientational motions of molecules.[42,46] By classifying molecules in configurations into subensembles with some features of their local environments, the local-structure effects on the intermolecular and unstable INM spectra of water have been examined.[46,47]

In the model of water molecules with flexibility, the bending and stretching motions of molecules produce the

a)Author to whom correspondence should be addressed. Electronic mail: tmw@faculty.nctu.edu.tw

intramolecular vibrational spectrum. Besides the unstable branch, the stable INM spectrum of a flexible water model is well separated in frequency into the intermolecular and intramolecular regimes, with the latter also resolvable into the bending and stretching INMs by their frequencies.[44,45] In Ref. 45, the stretching INMs were further decomposed into the symmetric and antisymmetic modes; however, the two kinds of modes are strongly overlapped in frequency. Also, the intermolecular interactions and the local environment of a molecule break the symmetry of the molecule, which makes the assignments of the symmetric and antisymmetic stretching INMs meaningless.

In this paper, by the INM analysis, we investigate the intermolecular and intramolecular vibrations in two SPC/E flexible water models. Instead of the molecular point of view, we consider from the atomic viewpoint, in which atoms are regarded as the basic units, so that the *INM* spectrum of each model is contributed from the *O* and *H* atoms. The paper is organized as the following. In Sec. II, we first introduce the two flexible models and then their structures and H-bond patterns generated by simulations are compared. In Sec. III, the INM formalism based on the atomic point of view are given, including the IPRs formulated, respectively, for the O- and H-atom and molecule, and the subensemble approach for investigating the local-structure effects on the INM spectrum. The results and discussions are given in Sec. IV. Our conclusions are given in Sec. V.

II. FLEXIBLE WATER MODEL AND SUBENSEMBLES

A. Flexible SPC models

We consider two flexible SPC water models, in which each molecule carries three point charges with q_O and q_H at the positions of the O- and H-atoms, respectively. The total interaction V in each model includes intermolecular $V_{\rm Inter}$ and intramolecular $V_{\rm Intra}$ terms, where $V_{\rm Inter}$ is the same for the two models but $V_{\rm Intra}$ is different. In the SPC model,[48] $V_{\rm Inter}$ consists of Coulombic potentials between any pairs of charges from two molecules and the Lennard-Jones (LJ) potential between the O atoms, with the parameter values referred to Ref. 48. In the flexible SPC model, the two OH bonds of a water molecule generally oscillate in stretching around a bond length $r_e = 1$ Å and the HOH bond angle makes a bending oscillation around a value θ_e close to the tetrahedral angle 109.4°. In the next, we describe separately the intramolecular interactions in each model:

(i) *Model I*: In the model proposed by Toukan and Rahman,[49] the stretching motion of each OH bond is described by the Morse potential and the bending motion of bond angle is by a harmonic term of the HH distance around its equilibrium value. Besides these two, the model contains linear couplings between the stretching motions of the two OH bonds and between each OH-bond stretching and the bending of bond angle. In this model, referred as *Model I* in this paper, the intramolecular interactions of a molecule are expressed as[50–52]

$$V_{Intra}^{(I)} = \sum_{l=1}^{2} D\left[1-\exp(-a\Delta r_l)\right]^2 + \frac{1}{2}k_\theta(\Delta r_3)^2 + k_{r\theta}\Delta r_3(\Delta r_1+\Delta r_2) + k_{rr}\Delta r_1\Delta r_2, \quad (1)$$

with $\Delta r_1 = r_{OH_1} - r_e$, $\Delta r_2 = r_{OH_2} - r_e$, and $\Delta r_3 = r_{H_1H_2} - r_{ae}$, where r_{OH_1}, r_{OH_2}, and $r_{H_1H_2}$ are the three distances between any two atoms in a molecule, with the two H atoms denoted as H_1 and H_2, and r_{ae} is the equilibrium distance between the two H atoms sustaining a bond angle θ_e. D and a are the parameters of the Morse potential. The force constants k_θ, k_{rr}, and $k_{r\theta}$ describe the harmonic potential of bond angle, the coupling between two stretching motions and the stretching-bending coupling, respectively. Referred from Ref. 52, the parameter values are summarized in Table I. This flexible model has been used to study the IR spectra of bulk water,[53,54] from the supercooled regime to the liquid-vapor coexistence at high temperatures, and the spectra of confined water in carbon nanotubes[55,56] and in mixtures.[57]

(ii) *Model II*: In a simple flexible SPC model, without any coupling between the stretching and bending motions, only a harmonic bending of bond angle and an anharmonic stretching of each OH bond are involved.[58] We refer this model as *Model II* in this paper and its intramolecular interactions are written as

$$V_{Intra}^{(II)} = \sum_{i=1}^{2}\left[k_{OH}(\Delta r_i)^2 + \alpha k_{OH}(\Delta r_i)^3\right] + k_{HOH}(\Delta\theta)^2, \quad (2)$$

where $\Delta\theta = \theta - \theta_e$ and Δr_i ($i = 1$ and 2) are defined as in *Model I* and k_{OH} and k_{HOH} are the force constants for harmonic stretching and bending oscillations, respectively. The parameter α describes the anharmonicity of the OH stretching relative to its harmonic potential. This flexible model is characterized by the appearance of cavities in the local structures of molecules as the system density is decreased. Also, the vibrational spectra of this model have been studied.[58] The parameter values in our study are listed in Table I, where the k_{OH} and α values

TABLE I. Parameters in intramolecular interactions of *Model I* and *II*. The values of the parameters in *Model I* and *II* are referred from Refs. 52 and 58, respectively, except for the k_{HOH} value being reduced to one quarter of the referred data. The force constants k_θ, $k_{r\theta}$, k_{rr}, and k_{OH} are in the unit of kJ mol^{-1} Å^{-2} and the unit of k_{HOH} is kJ mol^{-1} rad^{-2}.

Model I	Model II
$\theta_e = 109.47°$	$\theta_e = 109.43°$
$r_e = 1$ Å	$r_e = 1$ Å
$r_{ae} = 1.633$ Å	$k_{OH} = 2288.90$
$a = 2.567$ Å^{-1}	$k_{HOH} = 208.41$
D = 426.43 kJ mol^{-1}	$\alpha = -1.65$Å^{-1}
$k_\theta = 1375.05$	
$k_{r\theta} = -884.78$	
$k_{rr} = 467.38$	

are the same as in Ref. 58 but the k_{HOH} value is reduced to one quarter of the referred data such that the peak position of the calculated bending band is close to that observed in the IR spectrum of water at room temperature.[2]

In our MD simulation for each model, we confined 256 water molecules in a cubic box of length $L = 19.712$ Å at $T = 300\ K$ and density $\rho = 1$ g/cm^3. The leap-flog algorithm[59] was used to integrate the equations of motion with a time step of 0.2 fs. Subject to the periodic boundary conditions and the image convection, the long-range Coulombic interactions were treated with the Ewald summation method[60] and the LJ potential between the O atoms was truncated at a half of box length. The molecules were initially positioned in a fcc lattice and their velocities were randomly distributed. The system was ensured to get equilibrium in the first 300 ps of each simulation. Then, we started to collect data at every five time steps for total 10^6 configurations.

The structures of the two flexible models are compared by their radial distribution functions $g_{OO}(r)$, $g_{OH}(r)$, and $g_{HH}(r)$ and with the corresponding distributions of the rigid SPC/E model at the same density and temperature; the results are shown in Fig. 1. Our results indicate that the two flexible models have almost the same radial distribution functions of the OO, OH, and HH atomic pairs. However, compared with the rigid model, the local structures of the flexible model have some changes due to the intramolecular interactions such that the three radial distribution functions have a higher first peak occurring at a shorter distance and a deeper first minimum. For individual molecules in the two flexible models, the OH bond length in average is prolonged to 1.02 Å and the HOH bond angle is somewhat compressed to the most probable value at 104.9°, close to the bond angle of a realistic water molecule.

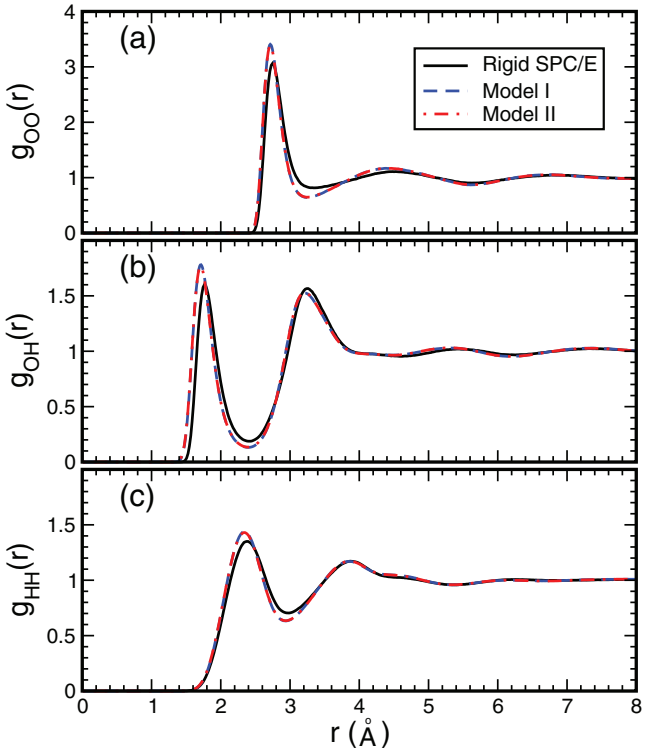

FIG. 1. Radial distribution functions of SPC/E models at $T = 300$ K and $\rho = 1$ g/cm^3: (a) $g_{OO}(r)$, (b) $g_{OH}(r)$, and (c) $g_{HH}(r)$. The solid lines are for the rigid model. The dashed and dotted-dashed lines are for *Model I* and *II* of flexible molecules, respectively.

B. Subensembles of local structures

To explore the local structures in simulated liquids, we have performed two structural analyses: the Voronoi tessellation method[61] and the H-bond configuration.[46] By the two analyses, the local structures of the rigid SPC/E model have been given in Ref. 46. In the following, we describe the two methods and the analyzed results of the two flexible SPC/E models.

1. Voronoi tessellation method

The Voronoi tessellation is a standard method to investigate local structures of water.[46,62–67] We applied this method for the O atoms in each flexible model. In this analysis, each molecule is associated with a Voronoi polyhedron (VP), which geometry is determined by the arrangement of its nearest neighbors. With the definition given in Ref. 46, a parameter η, called the asphericity, is a measurement for the geometric deviation of the VP from a sphere, which has $\eta = 1$. With the nearest neighbors in the tetrahedral arrangement as in the ice I_h structure, the VP of the molecule is strongly deviated from a sphere and its η value is 2.25. For molecules in liquid water, the η values are between the two extremes, with a general trend that the local structures of molecules with a larger η value are more tetrahedral-like.

Evidenced in Fig. 2, the asphericity distributions of the two flexible models are almost equivalent. As compared with the rigid model, the maximum in the asphericity distribution of a flexible model shifts toward a larger η value, indicating that the flexibility of water molecules favors the local structures of molecules to be tetrahedral-like. By dividing the asphericity distribution into four regions (shown in Fig. 2),

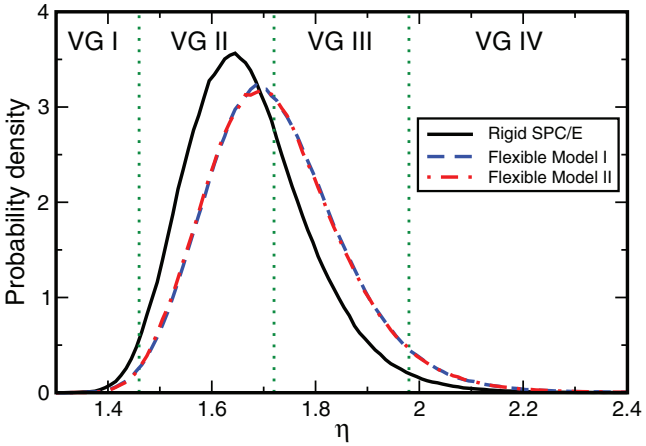

FIG. 2. Asphericity distribution of SPC/E model. The solid line is for the rigid model. The dashed and dotted-dashed lines are for *Model I* and *II*, respectively. By the dot vertical lines at $\eta = 1.46$, 1.72, and 1.98, the distribution of each model is divided into four regions, with each corresponding to a VG.

TABLE II. Average molecular fractions of subensembles for *Model I* and *Model II*. The subensembles are either four VGs or ten H-bond configurations. For each kind of classification, the fractions of all subensembles are summed to be unit. For H-bond configurations, the results are evaluated with the H-bond definition of both energetic and OOH-angle criterions described in the text and the results evaluated with the energetic criterion only are given in the parentheses.

Model	Molecular fraction χ_S of subensmble S				
	Subensembles classified by Voronoi group				
	VG I ($\eta < 1.46$)	*VG II* ($1.46 < \eta < 1.72$)	*VG III* ($1.72 < \eta < 1.98$)	*VL IV* ($1.72 < \eta$)	
Model I	0.0065	0.5020	0.4480	0.0435	
Model II	0.0060	0.5054	0.4448	0.0438	
	Subensembles classified by H-bond configuration				
	D2A3	D3A2	D2A2	D1A2	D2A1
Model I	0.0269 (0.0516)	0.0003 (0.0163)	0.4684 (0.5266)	0.1533 (0.1315)	0.2145 (0.1879)
Model II	0.0271 (0.0508)	0.0003 (0.0163)	0.4726 (0.5285)	0.1536 (0.1326)	0.2138 (0.1881)
	D0A2	D1A1	D2A0	D0A1	D1A0
Model I	0.0135 (0.0076)	0.1004 (0.0672)	0.0063 (0.0033)	0.0129 (0.0057)	0.0035 (0.0014)
Model II	0.0130 (0.0074)	0.0982 (0.0661)	0.0062 (0.0033)	0.0120 (0.0055)	0.0032 (0.0014)

with the same partitions for the rigid model as before,[66,46,47] we classify water molecules in each flexible model into four groups, assigned as Voronoi Group (VG) I to IV with increasing their η values. For the two flexible models, the average molecular fractions χ_S of the four VGs are given in Table II. Compared with the rigid model,[46] the χ_S values of VG I and II decrease but those of VG III and IV increase due to the flexibility of molecules.

The local structures of the four VGs are characterized by their radial distribution functions. Again, almost the same for the two flexible models, the results calculated for *Model II* are shown in Fig. 3 and the radial distribution functions of each VG have behaviors similar as those of the rigid model. A point worth noticing is that, rather than a plateau as for the rigid model, the second shell in $g_{OO}(r)$ of VG I is well observed for the flexible model and occurs in a regime where the corresponding distributions of the other three VGs have a minimum. Also, the maxima in $g_{OH}(r)$ and $g_{HH}(r)$ of VG I change from the first shell to the second. According to these features, the local structures of VG I are suggested to be resulted from some interstitial molecules.[66]

2. H-bond configuration

The local structures in water are strongly determined by its H-bond network. Generally, there are two approaches for defining a H-bond.[68] In the energetic definition, the shortest-distance O-H pair from two water molecules is considered to connect with a H-bond as the potential energy of the molecular pair is lower than a cutoff E_{HB}, which is usually set near the minimum in the potential-energy distribution of every molecular pairs in the liquid, so that the value of E_{HB} depends on the model studied. In the geometric definition, a H-bond in the simplest version is determined by a single criterion on the O-O distance between two molecules, with the first minimum of the $g_{OO}(r)$ function as the cutoff. Besides this distance restriction, a more popular version of the H-bond definition is to impose an extra criterion on the angle between the OH bond of a molecule and the O-O direction with respect to

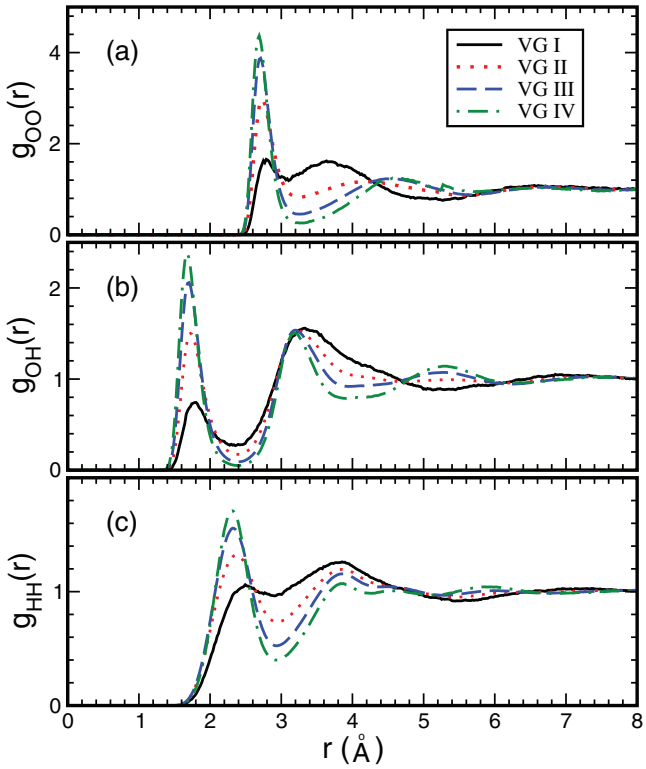

FIG. 3. Radial distribution functions of the four VGs for *Model II*: (a) $g_{OO}(r)$, (b) $g_{OH}(r)$, and (c) $g_{HH}(r)$. In each panel, the solid, dotted, dashed, and dotted-dashed lines are for VG I, II, III, and IV, respectively.

another molecule. By requiring this OOH angle to be smaller than a cutoff θ_c, mostly chosen at 30°, the H-bond is roughly directional along the OH bond. Though different definitions of a H-bond have been adopted, the analyzed structures and dynamics of liquid water are generally consistent in quality.

In this paper, we adopt a combination of the energetic and geometric definitions. That is, we define a H-bond with two criterions: (i) the energetic definition with $E_{HB} = -12$ kJ mol^{-1} and (ii) the cutoff $\theta_c = 30°$ for the OOH angle. As usual, two molecules connected by a H-bond are named as the donor (D) and acceptor (A), which donates and accepts the proton intermediate between the two O atoms, respectively. We denote the H-bond configuration of a molecule donating n and accepting m H-bonds as DnAm.[46] According to this definition, we find nine possible H-bond configurations for *Model I* and *II*; listed in Table II, their average molecular fractions calculated for the two models are rather similar. The D2A2, molecules with four H-bonds, is the most probable one. The average number of H-bonds per molecule is close to 3.37. On the other hand, for H-bonds with the energetic definition only, the molecular fractions are also given in Table II; the D3A2 molecules are found and the average H-bond number per molecule increases to 3.57. Thus, imposing the OOH angle criterion into the H-bond definition reduces the D3A2 fraction to almost vanish.

We have examined the distribution of the H-bond configurations for molecules in each VG. The results are still similar for the two flexible models so that we only show those of *Model II* in Fig. 4. Qualitatively, the correlations between the H-bond configurations and the VGs are similar for the flexible and rigid SPC/E models.[46] D2A2 is the most probable configuration for VG II, III, and IV but D1A1 is for VG I.

III. INM FORMALISM FOR FLEXIBLE MODELS OF WATER

With the generated configurations, we have calculated their Hessian matrices,[42] the second derivatives of total potential energy V with respect to the mass-weighted atomic coordinates $z_{k\gamma\mu} = \sqrt{m_\gamma} r_{k\gamma\mu}$, where m_γ is the mass of atom γ and $r_{k\gamma\mu}$ is the Cartesian coordinate in the μ direction of atom γ in molecule k, with $\gamma = O, H_1, H_2$ for the three atoms of each molecule. For a configuration $\boldsymbol{R}$ of N flexible water molecules, diagonalizing the $9N \times 9N$ Hessian matrix provides the *INM* frequencies $\omega_\alpha(\boldsymbol{R})$, $\alpha = 1, \ldots, 9N$, and the *INM* eigenvectors, which components are expressed as $e^\alpha_{k\gamma\mu}$ for the αth *INM*. The *INMs* are distinguished into the stable and unstable modes by their real and imaginary frequencies, respectively. The three eigenvector components $e^\alpha_{k\gamma\mu}$, with $\mu = x, y, z$, form a three-dimensional displacement $\vec{e}^{\,\alpha}_{k\gamma}$ of atom γ in molecule k in the *INM*. Each *INM* eigenvector is normalized so that the $3N$ displacements of atoms in this *INM* follow a sum rule,

$$\sum_{k=1}^{N} \sum_{\gamma=O,H_1,H_2} \left|\vec{e}^{\,\alpha}_{k\gamma}\right|^2 = 1, \tag{3}$$

with

$$\left|\vec{e}^{\,\alpha}_{k\gamma}\right|^2 = \sum_{\mu=x,y,z} e^\alpha_{k\gamma\mu} \cdot e^\alpha_{k\gamma\mu}. \tag{4}$$

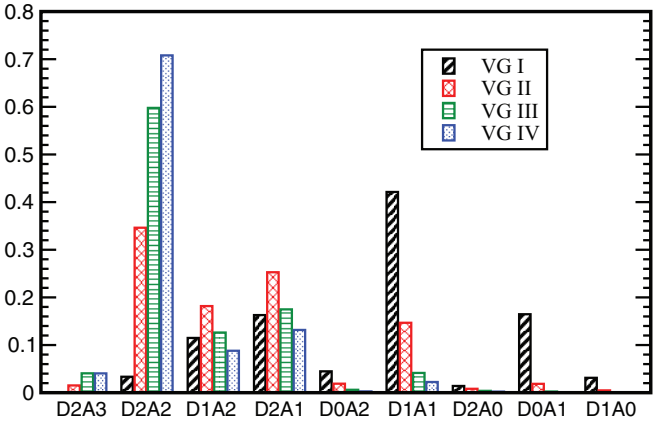

FIG. 4. Distribution of H-bond configuration for molecules in each VG of *Model II*. For a VG, the distribution is presented by bars with the same symbol and color, with the bars summed to be a unit. The distribution of each VG is shown for nine H-bond configurations, with the fraction of D3A2 almost zero for all VGs.

A. *INM* density of states

With the *INM* frequencies, the density of states (DOS) of *INMs* is expressed as

$$D(\omega) = \left\langle \frac{1}{9N} \sum_{\alpha=1}^{9N} \delta(\omega - \omega_\alpha(\boldsymbol{R})) \right\rangle, \tag{5}$$

where the angular brackets denote an ensemble average over liquid configurations. In the atomic point of view, we regard the *INM* DOS as contributions from the O and H atoms. To separate out the contributions of the two species, we define the atomic projector of the αth *INM* as

$$P_{\alpha,\gamma} = \sum_{k=1}^{N} \left|\vec{e}^{\,\alpha}_{k\gamma}\right|^2, \tag{6}$$

where γ is either O, H_1, or H_2. The eigenvector normalization gives the relation

$$P_{\alpha,O} + P_{\alpha,H_1} + P_{\alpha,H_2} = 1. \tag{7}$$

In terms of the atomic projectors, the atomic contribution to the *INM* DOS is defined as

$$D_\gamma(\omega) = \left\langle \frac{1}{9N} \sum_{\alpha=1}^{9N} P_{\alpha,\gamma} \delta(\omega - \omega_\alpha(\boldsymbol{R})) \right\rangle. \tag{8}$$

After the ensemble average, the contributions of the two H atoms of each molecule are equivalent and therefore, at this level, the subscript γ is reduced to either O or H. Thus, $D(\omega) = D_O(\omega) + 2D_H(\omega)$, where $D_O(\omega)$ and $D_H(\omega)$ are the contributions to the *INM* DOS from the O and one H atom of each molecule, respectively.

B. Inverse participation ratio

One measure for localization of normal modes is the IPR.[41,42] Based on the idea of IPR, we formulate the IPRs of the *O*- and *H*-atoms participated in the αth *INM*, respectively, as

$$R_{\alpha,O} = \left(\frac{1}{P_{\alpha,O}^2} \sum_{k=1}^{N} \left| \vec{e}_{kO}^{\alpha} \right|^4 \right)^{-1} \tag{9}$$

and

$$R_{\alpha,H} = \left[\frac{\sum_{k=1}^{N} \left(\left| \vec{e}_{kH_1}^{\alpha} \right|^4 + \left| \vec{e}_{kH_2}^{\alpha} \right|^4 \right)}{(P_{\alpha,H_1} + P_{\alpha,H_2})^2} \right]^{-1}. \tag{10}$$

As so defined, $R_{\alpha,O}$ and $R_{\alpha,H}$ measure the numbers of *O* and *H* atoms involved in the INM, respectively. For a completely delocalized *INM,* which eigenvector is equally shared among the 3*N* atoms, $|\vec{e}_{k\gamma}^{\alpha}|^2 = 1/3N$ for each atom and $P_{\alpha,O} = P_{\alpha,H_1} = P_{\alpha,H_2} = 1/3$ so that $R_{\alpha,O}$ and $R_{\alpha,H}$ are equal to *N* and 2*N*, respectively. On the other hand, if an INM is localized at a single atom, either *O* or *H*, both $P_{\alpha,\gamma}$ and $R_{\alpha,\gamma}$ are one for this species of atom or are zero otherwise.

After averaging the IPRs over a small *INM* frequency window, the number of atomic species γ participated in the *INMs* with ω is given as

$$R_{\gamma}(\omega) = \frac{1}{9N D(\omega)} \left\langle \sum_{\alpha=1}^{9N} R_{\alpha,\gamma} \delta(\omega - \omega_{\alpha}(\boldsymbol{R})) \right\rangle, \tag{11}$$

where γ can be either *O* or *H*. Similarly, we define the IPR of molecules as

$$R_{\alpha,M} = \left[\sum_{k=1}^{N} \left(\sum_{\gamma=O,H_1,H_2} \left| \vec{e}_{k\gamma}^{\alpha} \right|^2 \right)^2 \right]^{-1}, \tag{12}$$

where the sum rule in Eq. (7) has been used. This definition ensures that $R_{\alpha,M}$ equals one or *N* for a completely localized or delocalized *INM*, respectively. Thus, the number of molecules participated in the *INMs* with ω can be obtained via Eq. (11) by generalizing the subscript γ to include *M* for the case of molecule.

C. *INM* DOS of a subensemble

In Sec. II, we have classified molecules in configurations into subensembles of either VGs or H-bond configurations. For each kind of classification, we define a selector $\Theta_k(S)$ for each molecule such that $\Theta_k(S)$ is one for molecules belonging to a subemsemble indexed with *S* or zero otherwise.[46,47] Thus, for a configuration, the number of molecules in subensemble *S* is given as

$$N_S = \sum_{k=1}^{N} \Theta_k(S). \tag{13}$$

With $\Theta_k(S)$, the INM atomic projector for molecules in subensemble *S* is defined as

$$P_{\alpha,\gamma}^{S} = \sum_{k=1}^{N} \left| \vec{e}_{k\gamma}^{\alpha} \right|^2 \Theta_k(S). \tag{14}$$

The projectors of subensembles are subject to two sum rules:

$$\sum_{S} P_{\alpha,\gamma}^{S} = P_{\alpha,\gamma} \tag{15}$$

and

$$\sum_{\alpha=1}^{9N} P_{\alpha,\gamma}^{S} = 3N_S. \tag{16}$$

It is easy to understand the first sum rule, in which the summation runs for all subensembles characterized by a certain feature of local structure. In the second sum rule, the equality is based on the completeness of the 9*N* *INM* eigenvectors of each configuration and the projector $P_{\alpha,\gamma}^{S}$ involves $3N_s$ components of an *INM* eigenvector, where the factor three comes from the x, y, z components of each atom.

Similarly, with the projector $P_{\alpha,\gamma}^{S}$, the average contribution of one atom of species γ in subensemble *S* to the *INM* DOS is given as

$$D_{\gamma}^{(S)}(\omega) = \left\langle \frac{1}{3N_S} \sum_{\alpha=1}^{9N} P_{\alpha,\gamma}^{S} \delta(\omega - \omega_{\alpha}(\boldsymbol{R})) \right\rangle. \tag{17}$$

Due to Eq. (16), $D_{\gamma}^{(S)}(\omega)$ is normalized. By using Eq. (15), one can verify

$$D_{\gamma}(\omega) = \frac{1}{3} \sum_{S} \chi_S D_{\gamma}^{(S)}(\omega), \tag{18}$$

where $\chi_S = N_S/N$ is the average molecular fraction of subensemble *S*.

D. Related to velocity autocorrelation function

Through a series of approximations,[52,53] the vibrational spectrum of water is related to the power spectra $Z_{\gamma}(\omega)$ of the normalized velocity autocorrelation functions (VACFs) $C_{v,\gamma}(t)$ of *H* and *O* atoms. The INM and VACF approaches are correlated via a correspondence between the atomic power spectrum $Z_{\gamma}(\omega)$ and the stable branch of $D_{\gamma}(\omega)$, with both normalized. The atomic power spectra are usually considered as a result of full interactions. Obtained via a long-time MD simulation, the VACFs contain the motional narrowing effect; however, during the simulation the local structure of a molecule changes frequently so that the structural information is averaged out. Thus, this approach is unavailable to extract the structural effects on vibrational spectrum of water. On the other hand, without the motional narrowing effect, the *INM* DOS is in the inhomogeneous limit.[69] Hence, the INM formalism for subsensembles derived in this section paves the way for studying the local-structure effects on the INM spectrum of water.[46,47] Comparisons of the INM and VACF approaches for the two flexible models are presented in Sec. IV.

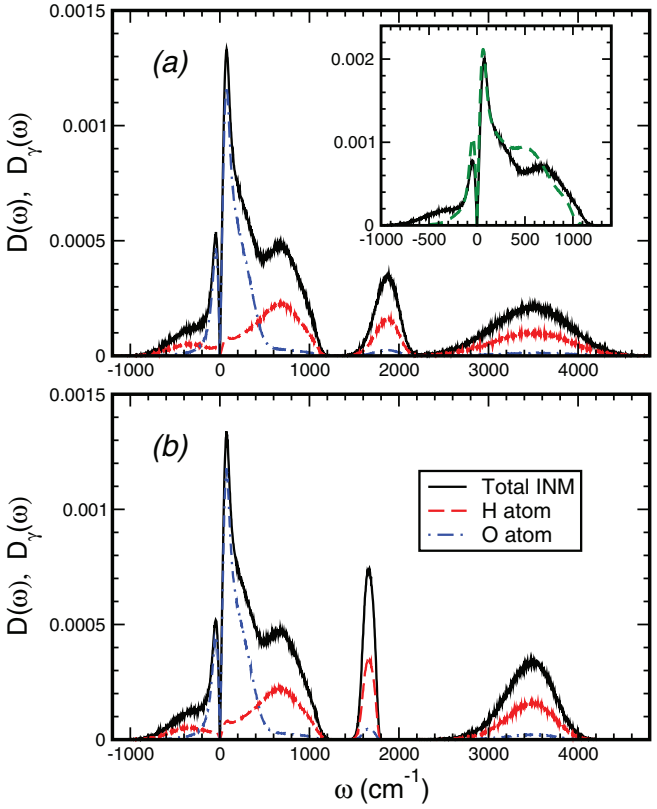

FIG. 5. INM DOS, $D(\omega)$, and its atomic contributions, $D_\gamma(\omega)$, for (a) *Model I* and (b) *Model II* at T = 300 K and $\rho = 1$ g/cm^3. The black solid lines are for the INM DOS. The red dashed and blue dotted-dashed lines are for the H- and O-atom contributions, respectively. The inset in (a) shows the comparison of the intermolecular and unstable branches calculated for *Model I* (black-solid line) with those of the rigid model[46] (green dashed line) at the same density and temperature, where both curves are normalized.

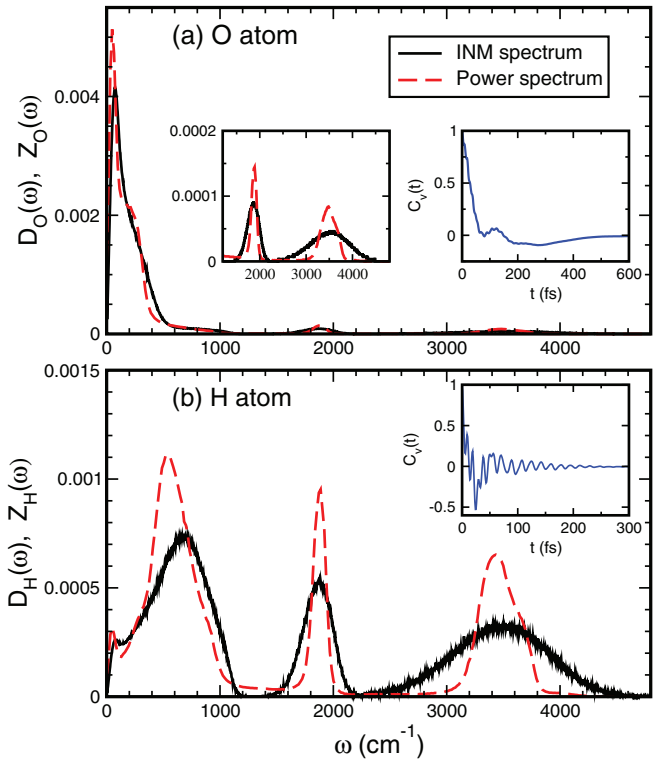

FIG. 6. Stable INM spectrum of $D_\gamma(\omega)$ and the atomic power spectrum $Z_\gamma(\omega)$ for *Model I*: (a) O atom and (b) H atom. In each panel, the solid line is for the stable branch of $D_\gamma(\omega)$ and the dash line is for $Z_\gamma(\omega)$ obtained via the VACF $C_{v,\gamma}(t)$ shown in the inset, with both curves normalized. In an inset in (a), the bending and stretching portions of the O-atom contribution are enlarged for a clear view.

IV. RESULTS AND DISCUSSIONS

A. *INM* spectrum

The *INM* DOS, $D(\omega)$, and its atomic contributions, $D_\gamma(\omega)$, of the two flexible models are shown in Fig. 5, in which the stable and unstable branches are plotted along the positive- and negative-frequency axes, respectively. For each model, the stable-*INM* spectrum is clearly separated into three frequency regimes corresponding to the intermolecular, bending and stretching vibrations. Almost identical for the two flexible models, the intermolecular portion and the unstable branch of the flexible model are compared with the *INM* DOS of the rigid SPC/E model[46] in the inset in Fig. 5(a). But, the intramolecular *INM* spectra of the two flexible models differ in shape and frequency regime. The comparisons between the stable branch of $D_\gamma(\omega)$ after normalized and the atomic power spectrum $Z_\gamma(\omega)$ are presented in Figs. 6 and 7 for *Model I* and *II*, respectively. In the following, we discuss separately the *INM* spectra of the flexible models in different frequency regimes.

1. Intermolecular INMs and the unstable branch

At frequencies less than 1200 cm^{-1}, the stable *INM* spectrum of the flexible model is associated with the

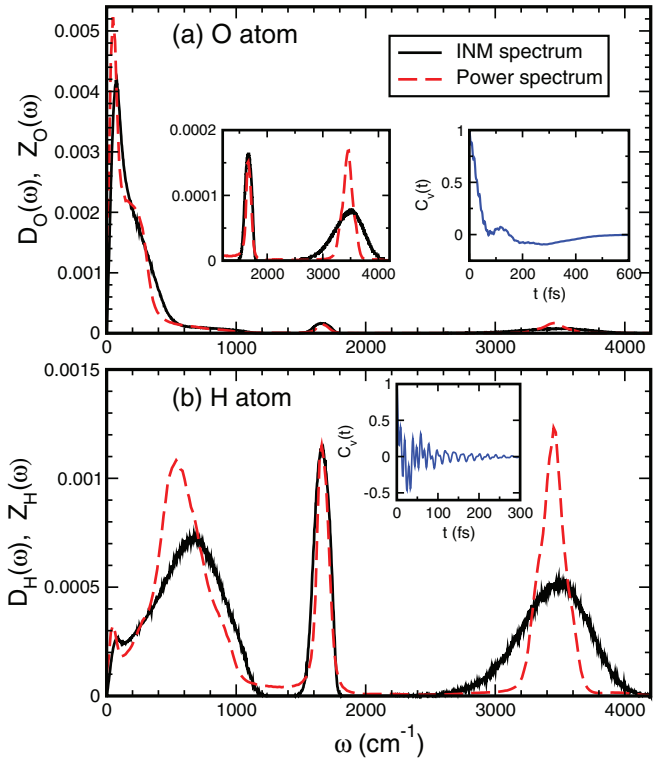

FIG. 7. The same as in Fig. 6, except for *Model II*.

intermolecular vibrations. Near 75 cm^{-1}, we observe a sharp peak, which comes from the 60 cm^{-1} peak as molecules are rigid.[47] This peak is strongly dominated by *O* atoms and this is consistent with the assignment of the peak as the O-O-O bending of the triplets of water molecule.[47,70] Dominated at low frequencies, the *O*-atom contribution monotonically decays with ω from this peak up to 500 cm^{-1}. For the two flexible models, the power spectrum $Z_O(\omega)$ exhibits a maximum close to 50 cm^{-1} and a shoulder around 200 cm^{-1}, corresponding to the two bands observed in Raman spectrum of water;[6] however, the two bands merge together in the *INM* spectrum. Beyond 500 cm^{-1}, $D(\omega)$ becomes dominated by *H* atoms and a second peak is observed around 670 cm^{-1} but the corresponding peak in $Z_H(\omega)$ appears roughly at 550 cm^{-1}. From the molecular viewpoint,[45] this second peak is associated with the orientational motions of molecules. In the orientational contribution, the *INM* displacements associated with *H* atoms have larger amplitudes than those associated with *O* atoms. This explains why the intermolecular spectrum beyond 500 cm^{-1} is dominated by *H* atoms. Compared with the rigid model, the orientational contribution in the flexible model apparently shifts toward higher frequencies and, therefore, the upper limit of the intermolecular spectrum is extended about 100 cm^{-1}.

Due to the flexibility of molecules, the fraction of the unstable INMs is somewhat reduced (about 10.5%).[46] Much broader than the case of the rigid model and deformed from the triangular shape usually observed for the Lennard-Jones fluids,[71,72] the unstable *INM* spectrum of the flexible model is composed of two quite different components, a narrow one with a sharp peak near imaginary frequency of 50 cm^{-1} and a broad one with a weak peak close to 400 cm^{-1}, where the former is contributed by the *O* atoms and the latter is by the *H* atoms. Referred to the results in Ref. 45, the O-atom contribution is much associated with the translational motions of molecules and the H-atom contribution is with the orientational motions.

2. Intramolecular INMs

There are several common features in the intramolecular *INM* spectra of the two flexible modes: The spectrum is separated into the bending and stretching bands in different frequency regimes, the shape of each band is almost symmetric with respect to its maximum, and the *H*-atom contribution for each band is much dominated. The main differences for the two models lie in the frequency regimes of the bending and stretching bands and their bandwidths (FWHM). For *Model I*, the bending band has a maximum near 1850 cm^{-1} and a bandwidth about 310 cm^{-1}; for *Model II,* the maximum is near 1665 cm^{-1}, which is close to that observed in the IR spectrum of water,[2] and the bandwidth is roughly 150 cm^{-1}. For the stretching band, the maximum roughly occurs at the same position for both models, near 3500 cm^{-1}; however, the bandwidth of *Model I* is much broader than that of *Model II*, where the former and the latter are about 1000 cm^{-1} and 600 cm^{-1}, respectively. For *Model I*, the bending and stretching *INM* bands are so broad that they almost touch in tail. According to the results in Figs. 6 and 7 for both models, the maximum position of the bending band in the *INM* spectrum is close to that obtained from the atomic power spectrum, while the maximum position of the stretching *INM* band is about 100 cm^{-1} higher than that of the atomic power spectrum. However, except for the bending band of *Model II*, the bandwidths of the stretching and bending bands in the atomic power spectrum are much narrower (about 40 percents) than those in the INM spectrum. One reason for the broadness of the bending and stretching *INM* bands is the absence of the motional narrowing effect in the INM theory;[33,73] however, this effect is included in the atomic power spectrum.

B. Inverse participation ratio

The calculated $R_H(\omega)$, $R_O(\omega)$, and $R_M(\omega)$ for *Model I* and *II* are presented in the left and right columns in Fig. 8, respectively; the IPRs of intermolecular, bending and stretching *INMs* are plotted in separately panels for they are quite different in order of magnitude. Shown in Figs. 8(a) and 8(d) are the IPRs of the intermolecular and unstable *INMs,* which are almost equivalent for the two flexible models. On the other hand, except for small differences at some intermolecular frequencies, the $R_O(\omega)$ values are almost the same as those of $R_M(\omega)$. With increasing imaginary frequency, the three IPRs of the unstable INMs decay monotonically from an order of

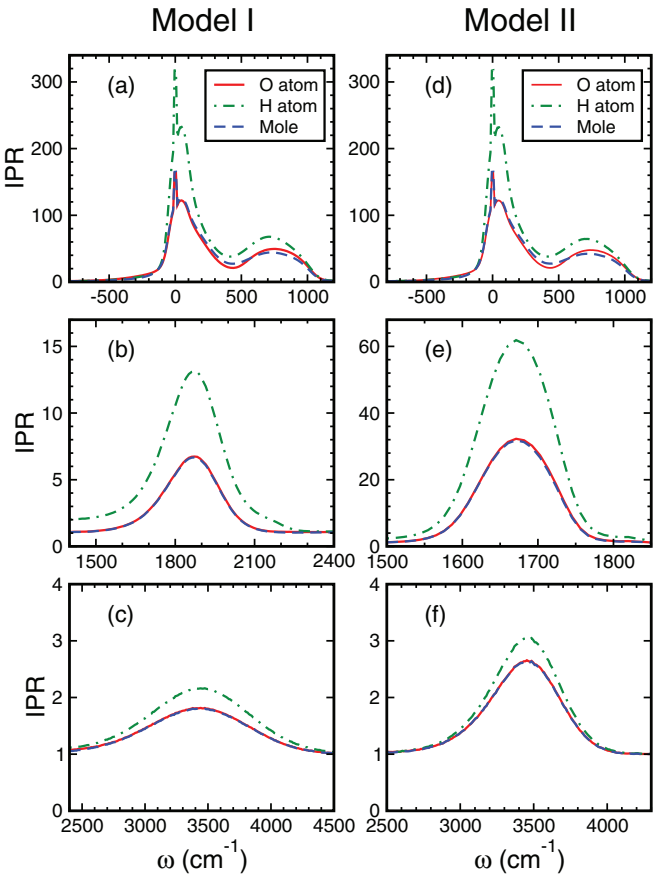

FIG. 8. IPRs of *INMs* in *Model I* (left column) and *Model II* (right column). In each panel, the red solid, green dotted-dashed, and blue dashed lines are the calculated results of $R_O(\omega)$, $R_H(\omega)$, and $R_M(\omega)$, respectively. For each column, the three panels from top to bottom are for the intermolecular and unstable, the bending, and the stretching INMs.

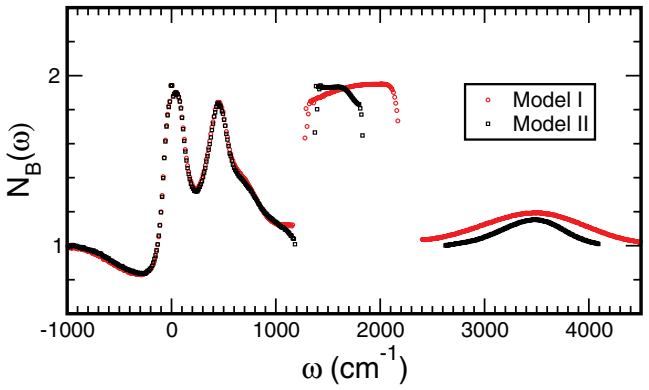

FIG. 9. Average number $N_B(\omega)$ of involved OH bond in each molecule participated in *INMs* with ω. The average number is obtained by Eq. (19) evaluated at frequencies where $D_O(\omega)$ is larger than 10^{-6} cm. The red circles and black squares are the results calculated for *Model I* and *II,* respectively.

hundred down to a value close to one, indicating that the behaviors of the unstable modes change from delocalized to extremely localized. In the intermolecular band, the variation of $R_M(\omega)$ with frequency is dramatic. At frequencies where the translational *INMs* are dominated, $R_M(\omega)$ decays from more than a hundred down to a minimum about 20 near 400 cm^{-1}. Beyond this minimum, where the *INMs* change behaviors to be associated with the rotational motions of molecules, $R_M(\omega)$ ascends to a maximum having a value of 50 and occurring roughly at 750 cm^{-1}, and then descends again to a value less than 2 at the band edge, where the *INMs* are quite localized.

With $R_H(\omega)$ and $R_O(\omega)$, the number of involved OH bond in each molecule that is participated in *INMs* can be estimated by their ratio

$$N_B(\omega) = \frac{R_H(\omega)}{R_O(\omega)}. \tag{19}$$

As $N_B(\omega) = 2$ or 1, two OH bonds or a single OH bond of each participated molecule are involved in the *INMs,* respectively. To avoid the frequencies where the *INMs* occur scarcely, we evaluate $N_B(\omega)$ only at frequencies with $D_O(\omega)$ larger than certain value (10^{-6} cm), and the results of the two flexible models are shown in Fig. 9. According to our results, both OH bonds of each participated molecule are involved in the INMs at very low imaginary frequencies; however, the number of involved OH bond decreases to one as the imaginary frequency increases up to near 140 cm^{-1}. At higher imaginary frequencies, $N_B(\omega)$ becomes less than one, indicating that the O atoms are more in number involved in these unstable *INMs* than the *H* atoms. This will be explored further in our future works.

For the intermolecular *INMs*, the variation of $N_B(\omega)$ with frequency is interesting. At ω less than 100 cm^{-1}, $N_B(\omega)$ is close to 2 and this is consistent with the assignment of the 75 cm^{-1} peak shown in Fig. 5 as the O-O-O bending: The two OH bonds of the central molecule of a water triplet are required for undergoing the O-O-O bending. For ω over 100 cm^{-1}, the behavior of $N_B(\omega)$ exhibits a minimum near 230 cm^{-1} and a maximum close to 450 cm^{-1}, with the extreme values about 1.3 and 1.8, respectively. Since the *INMs* around 230 cm^{-1} are associated with the stretching motions between O-O atoms,[6,70] we attribute the minimum in $N_B(\omega)$ as a result of these stretching motions, which do not require both OH bonds of a molecule at the same time. However, the appearance of the maximum near 450 cm^{-1} is somewhat bizarre, but intriguing. Around 450 cm^{-1}, both translational and orientational motions of molecules contribute the *INM* DOS; however, the orientational motions about the *x* and *z* principal axes of water molecule are more dominated than those about the y axis.[46] To explain the bizarre maximum and the decay of $N_B(\omega)$ with increasing ω to one at the band edge, we conjecture that the orientational motions about the three principal axes maybe involve different numbers of OH bond of each participated molecule but this needs some further studies.

The IPR variations in the bending and stretching INM bands are much simpler, by exhibiting a maximum near the center of each band and decaying to one at both band edges. However, the maximum $R_M(\omega)$ values of the bending and stretching bands are different and depend on the flexible model. Indicated in Figs. 8(b) and 8(e) for the bending band, the maximum of $R_M(\omega)$ is 6 or 7 for *Model I* but can be as large as 30 for *Model II*. Relative to the total number of simulated molecules ($N = 256$), the bending *INMs* are expected to be localized in nature. For the stretching band shown in Figs. 8(c) and 8(f), the values of $R_M(\omega)$ are less than 3 for both models, which clearly indicates that all stretching *INMs* are extremely localized. This localization usually happens to the high-frequency vibrational modes of disorder systems.[37,74,75] Shown in Fig. 9 for both models, $N_B(\omega)$ is generally close to two for the bending *INMs* and around one for the stretching *INMs*. These results strongly indicate that in water the bending vibrations of molecules should require both OH bonds of each molecule but the stretching vibrations may not require both OH bonds of a molecule at the same time, with the two bonds oscillating independently. This indication suggests that the symmetric and antisymmetic assignments as in Ref. 45 are no longer valid for the stretching vibrations of water molecules in a disordered environment.

C. Local-structure effects on bending and stretching INM bands

By classifying molecules into subensemles as given in Sec. II B, the local-structures effects on the translational and orientational contributions to the intermolecular *INM* spectrum of the rigid SPC/E model have been reported in Ref. 46. Here, with the same methodology, we investigate the local-structure effects on the bending and stretching *INM* spectrum of flexible SPC/E models. We discuss only the H-atom contribution, although the conclusions given in the following can be also obtained by the O-atom contribution, which is in the same spectral shape as the H-atom contribution but much smaller in magnitude.

For the four VGs described in Sec. II B, their H-atom contributions $D_H^{(S)}(\omega)$ to the bending and stretching *INM* spectra are shown in Figs. 10(a) and 10(b) for *Model I* and *II*, respectively. Indicated by the results, the variation of $D_H^{(S)}(\omega)$ with the asphericity η of the VP constructed by the local structure of a molecule is generally consistent for the two

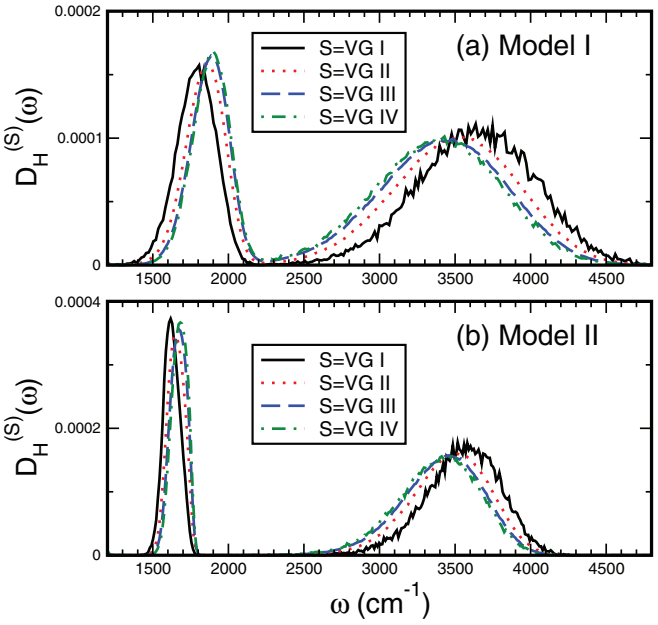

FIG. 10. H-atom contribution to the bending and stretching bands calculated for the four VGs: (a) *Model I* and (b) *Model II*. In each panel, the solid, dotted, dashed, and dotted-dashed lines are the results calculated for VG I, II, III, and IV, respectively.

flexible models. Clearly, for molecules with large η values, their local structures cause the bending band shifting toward higher frequencies (blue shift) but the stretching band shifting toward lower frequencies (red shift) so that the two bands approach each other. Physically, through interacting with its neighbors, the local environment of a molecule has a feedback on the structure of the molecule by changing the two OH bond lengths and the HOH bond angle and consequently influences the bending and stretching frequencies of the molecule. The agreement in the variation of $D_H^{(S)}(\omega)$ with η for the two flexible models is attributed to the same intermolecular interactions of the two models. Meanwhile, this agreement indicates that classifying molecules into subensembles by some feature of their environments is an effective method to examine the local-structure effect on the INM spectrum.

Certainly, the vibrational spectrum of water is strongly related to its H-bond network. Since the H-bond network in water is complicated and fluctuated, a key parameter that characterizes the cooperativity of the H-bonding on the vibrational spectrum, especially for the OH-stretching frequency of water molecule, is appealed. Generally, the stretching frequency of an OH bond is inversely proportional to the OH bond length,[76] which is influenced by the H-bonds attaching to the OH bond. But, the OH bond length of a molecule is also affected by other H-bonds connecting to this molecule and/or those connecting to the acceptor molecule conjugated to this OH bond through a H-bond. By studying water clusters, Ohno *et al.* proposed a *M* value that describes a superposition of the effects coming from other H-bonds connecting to the DA molecular pair, with some H-bonds contributed positively and some negatively.[76] They showed that the *M* value is a useful parameter for correlating the H-bonding patterns in regard to the molecular pair with the shifting in the stretching frequency of the OH bond, which belongs to the D and is connected with the A via a H-bond. Recently, with a similar idea, the *M* value is simplified as the number of the accepted H-bonds on the D subtracted out the number of the additional accepted H-bonds on the A; with this simplified *M* parameter, the OH-stretching spectroscopy of water molecules in cluster, liquid and ice and at liquid surface has been studied.[31]

We here consider each individual molecule as an identity, rather than an OH bond as for the *M* value. We have calculated the H-atom contribution to the bending and stretching *INM* bands for the subensembles of H-bond configurations listed in Table II. The calculated $D_H^{(S)}(\omega)$ of the bending band are shown in Fig. 11, in which the results with the same n_D are plotted in one panel, and the $D_H^{(S)}(\omega)$ of the stretching band are shown in Fig. 12, in which the results with the same $n = n_D + n_A$ are plotted together, where n_D and n_A are the numbers of donated and accepted H-bonds of a H-bond configuration, respectively. For each H-bond configuration, we define the average frequency of an INM band as the mean of $D_H^{(S)}(\omega)$ in a frequency range, within which only the INM band resides.[77] In such a way, the average bending and stretching frequencies, denoted as ω_{be} and ω_{st}, respectively, of the nine possible H-bond configurations given in Table II are obtained[78] and their values versus the total H-bond number n of a molecule are plotted in Figs. 13 and 14. Clearly indicated in the two figures, attaching one more H-bond, no matter donated or accepted, to molecules causes the bending

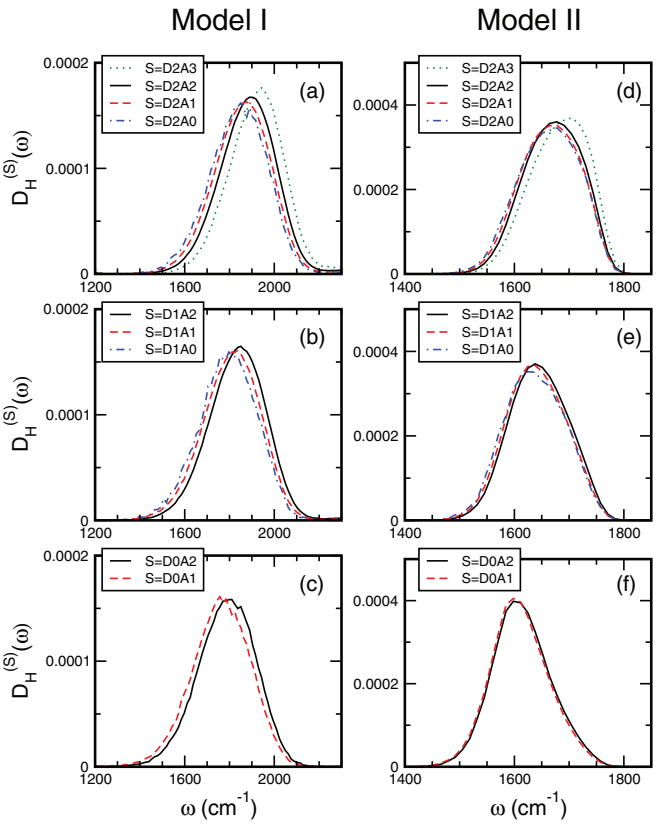

FIG. 11. H-atom contribution to the bending band calculated for subensembles of H-bond configuration: *Model I* (left column) and *Model II* (right column). In each column, the panels from top to bottom are for H-bond configurations with two, one, or zero donated H-bonds. In all panels, the dotted, solid, dashed, and dotted-dashed lines indicate the results of H-bond configurations with three, two, one, and zero accepted H-bonds, respectively.

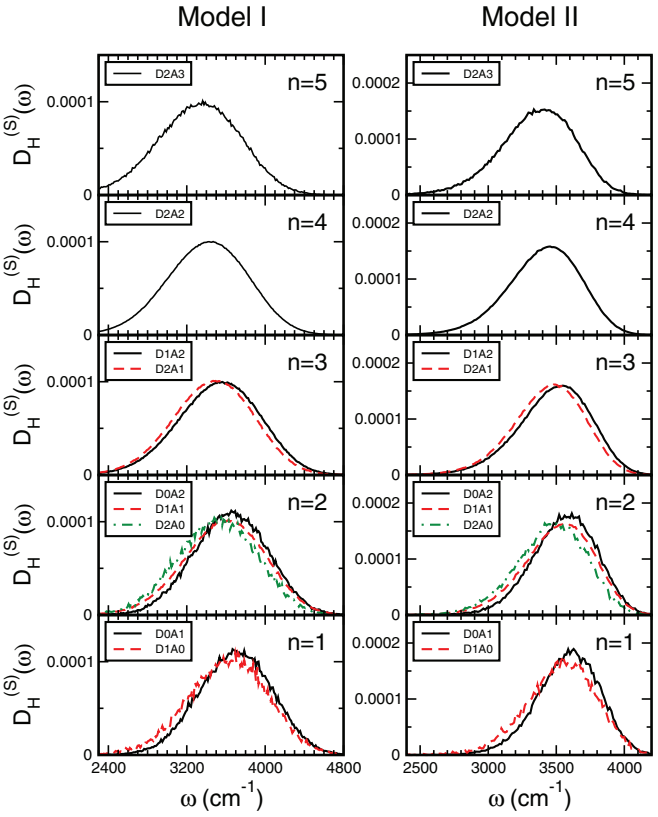

FIG. 12. H-atom contribution to the stretching band calculated for subensembles of H-bond configuration: *Model I* (left column) and *Model II* (right column). In each column, the panels from top to bottom are for H-bond configurations with total H-bond number n from 5 to 1. For $n = 5$ or 4, there is only one possible H-bond configuration. For $n = 3$, 2, or 1, the solid, dashed, and dotted-dashed lines are for the configurations with two, one, or zero accepted H-bonds, respectively.

band a blue shift (with ω_{be} increasing) and the stretching band a red shift (with ω_{st} decreasing); the amount of average shifting of each band depends on the type of the attaching H-bond and the flexible model. Especially, for H-bond configurations with $n \leq 4$ (except for D2A3), each of ω_{be} and ω_{st} shows linear dependences on n_D and n_A with different slopes that reply on the model. The details are addressed in the following.

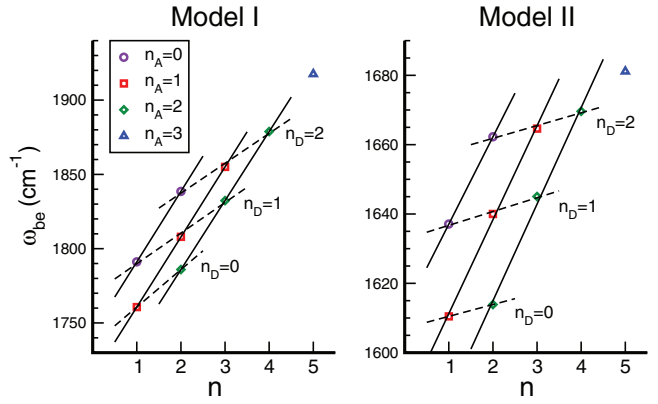

FIG. 13. Average bending frequency ω_{be} versus the total H-bond number n of a configuration: (a) *Model I* (left panel) and (b) *Model II* (right panel). The circles, squares, diamonds, and triangles are for the configurations with n_A from zero to three, respectively. The solid lines from left to right are the linear fit for each data set with $n_A = 0$, 1, or 2; the dash lines from top to bottom are the linear fit for the data set with $n_D = 2$, 1 or 0, respectively.

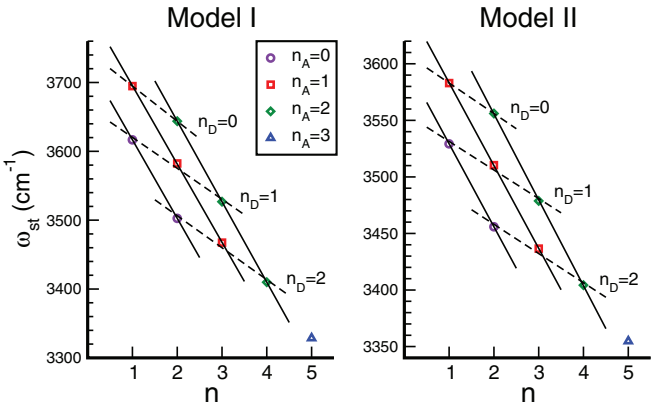

FIG. 14. Average stretching frequency ω_{st} versus the total H-bond number n of a configuration. The rest are the same as in Fig. 13, except that the dash lines from top to bottom are the linear fit for the data set with $n_D = 0$, 1 or 2, respectively.

In Fig. 13, we fit each ω_{be} data set ($n \leq 4$) with the same n_A or n_D by a linear function, which is shown by a solid or dash line, respectively. Generally, the increase of ω_{be} by one donated H-bond can be obtained by the average slope of the three solid lines in Fig. 13; the increase by one accepted H-bond can be given by the average slope of the three dash lines. As so estimated, the increase of ω_{be} for *Model I* is about 47 cm^{-1} by one donated H-bond and 21 cm^{-1} by an accepted one. For *Model II*, the increase of ω_{be} is about 27 cm^{-1} or 3.7 cm^{-1} by one donated or one accepted H-bond, respectively. Therefore, these data indicate that the shifting in the bending band caused by one donated H-bond is more than double of that by one accepted H-bond for *Model I*, but the ratio is more than seven times for *Model II*. Physically, this result can be realized as the following: Indicated by $N_B(\omega)$, the bending vibration of a molecule involves its two OH bonds at the same time and is more strongly related to the motions of H atoms than the O atom. Directly attaching to the H atoms, the donated H-bonds of a molecule conceivably result in an increase in the force constant of the bending vibration and, therefore, increase the bending vibrational frequency of the molecule. On the other hand, evidenced in Fig. 13, the bending frequency is also enhanced by the accepted H-bonds, which attach the O atom of the molecule. As shown in Fig. 11, this enhancement is detectable in $D_H^{(S)}(\omega)$ for *Model I* but weak for *Model II*. Thus, we consider *Model I* to be more flexible in the bending vibration than *Model II*.

Similarly, the decrease of ω_{st} by attaching one more donated or accepted H-bond to molecules can be obtained by the average slope of the solid or dash lines in Fig. 14, which are the linear fit for each data set of the H-bond configurations with the same n_A or n_D, respectively. The estimated decrease of ω_{st} caused by one donated or accepted H-bond is about 115 cm^{-1} or 47 cm^{-1} for *Model I* and about 74 cm^{-1} or 26 cm^{-1} for *Model II*, respectively. Hence, the ratio of the ω_{st} decrease by one donated H-bond to that by an accepted one is about 2.5 for *Model I* and 2.9 for *Model II*. Therefore, for both models, the red shift of the stretching band is dominated

by the donated H-bonds and partially contributed by the accepted H-bonds. For *Model II*, the accepted H-bonds play a more significant role to the stretching shift than the bending shift.

These results inspire us a physical picture for the stretching vibration of a water molecule. Though the two OH bonds of a molecule generally oscillate independently according to the results of $N_B(\omega)$, the stretching vibrational frequencies of a molecule are associated with all H-bonds attaching to it. In details, a donated H-bond, which directly exerts a force on the H atom, elongates effectively the attaching OH bond and, therefore, reduces significantly the stretching vibrational frequency of the OH bond. However, attaching to the heavy O atom which connects two OH bonds, an accepted H-bond of a molecule is supposed to elongate two OH bonds at the same time and results in, roughly, a half of the reduction in the stretching vibrational frequency caused by one donated H-bond. This picture is generally consistent with the results presented in Fig. 14 for the two flexible models.

The case of D2A3 molecules, which have five H-bonds, is intriguing. The average bending and stretching frequencies of D2A3 do not follow the linear dependences for the H-bond configurations with $n \leq 4$. Relative to the data of D2A2, the unique configuration with $n = 4$, the increase of ω_{be} or the decrease of ω_{st} caused by the fifth H-bond of D2A3 is found to be about the average of the frequency shift caused independently by one donated H-bond and that by one accepted H-bond according to the linear dependences for $n \leq 4$. Though it is interesting, to study further the effects of the fifth H-bond on the bending and stretching bands of water is beyond the scope of this paper. On the other hand, we have calculated the O- and H-atom contributions to the bending and stretching INM bands for the H-bond configurations with the H-bonds defined by the energetic definition only and the results calculated for the two models are almost the same as those with the H-bonds defined by both the energy and the OOH-angle criterions. Therefore, we remark that our conclusions about the H-bond effects on the bending and stretching INM bands of water are insensible to whether the OOH-angle criterion is included in the H-bond definition or not.

V. CONCLUSIONS

In terms of the INM analysis, we have investigated intermolecular and intramolecular vibrations in two flexible SPC/E water models, which have the same intermolecular but different intramolecular interactions. In an equivalence in the $g_{OO}(r)$, $g_{OH}(r)$, and $g_{HH}(r)$ functions and the average fractions of H-bond configurations, the two flexible models possess almost the same local structures and H-bond networks. Separated into several bands, the calculated INM spectra of the two models are almost identical in the unstable and intermolecular bands but differ in the bending and stretching intramolecular bands. From the atomic point of view, the O- and H-atom contributions to each INM band are calculated. In general, the O-atom contribution is dominated in the low-frequency unstable and intermolecular bands but the H-atom contribution spreads over the entire INM spectrum. In the absence of the motional narrowing effect, the atomic contributions to the bending and stretching INM bands are much broader than the corresponding atomic power spectra obtained by the VACFs but the predictions for the peak position of each band by the two approaches are generally consistent.

We have formulated three IPRs of INMs, respectively, for O- and H-atoms and molecules. In terms of the three IPRs, the average numbers of the three species that participated in the INMs are estimated for the two flexible models. For the two models, the numbers of participated O atoms and molecules are almost the same. The number of molecules participated in the intermolecular INMs exhibit two maxima at frequencies corresponding to the translational and orientational vibrations of molecules and the INMs around the two maxima are generally delocalized. Though the maximum number of molecules participated in the bending or stretching INMs depends on the flexible model, our results indicate that the bending INMs in the two models are generally localized in nature and the stretching INMs are strongly localized for sure. By the ratio of the IPR for H atoms to that for O atoms, we estimate the number of involved OH bond per molecule that is participated in the INMs. The estimated results indicate that both OH bonds of each molecule participated in the bending INMs are required but the two OH bonds of molecules participated in the stretching INMs oscillate independently; the latter leads us to conclude that the symmetric and antisymmetic assignments are no longer valid for the stretching vibrations of water molecules in liquids. In the intermolecular band, we find that both OH bonds of molecules participated in the low-frequency translational vibrations are involved and the situation also occurs with a large chance in a transition regime of frequency from the translational to orientational vibrations.

By subensembles of VGs and the H-bond configurations, we have examined the local-structure effects on the bending and stretching INM bands. In general, molecules with tetrahedral-like local structures favor the bending band having a blue shift and the stretching band having a red shift. Our results indicate that the shifts of the bending and stretching bands are dominated by the donated H-bonds and partly contributed by the accepted ones. In details, except for the rare molecules with five H-bonds, we find that the shifts in the average frequency of the bending and stretching INM bands are linearly proportional to the numbers of donated and accepted H-bonds attaching to a molecule, with the proportional constants of each band depending on the H-bond type and the model. Quantitatively, for the stretching band, the proportional constant due to the donated H-bond is more than double of that due to the accepted H-bond; this is applied for both models studied in this paper. For the bending band, the ratio of the proportional constant with the donated H-bond number to that with the accepted H-bond number is about two for *Model I* but about seven for *Model II* so that the shifting of the bending band for *Model II* is strongly associated with the donated H-bonds of a molecule. All of these conclusions are insensible to the H-bond definition, with the OOH-angle criterion or not.

ACKNOWLEDGMENTS

This work is supported by National Science Council, Taiwan under Grant No. NSC 102-2112-M-009-013-MY3. We thank the referees for comments and suggestions.

[1]H. J. Bakker and J. L. Skinner, Chem. Rev. **110**, 1498 (2010).
[2]J. E. Berti and Z. Lan, Appl. Spectrosc. **50**, 1047 (1996).
[3]J. B. Brubach, A. Mermet, A. Filabozzi, A. Gerschel, and R. Roy, J. Chem. Phys. **122**, 184509 (2005).
[4]N. Miura, H. Yamada, and A. Moon, Spectrochim. Acta, Part A **77**, 1048 (2010).
[5]G. E. Walrafen, M. S. Hokmabadi, and W. H. Yang, J. Chem. Phys. **85**, 6964 (1986).
[6]G. E. Walrafen, M. R. Fisher, M. S. Hokmabadi, and W. H. Yang, J. Chem. Phys. **85**, 6970 (1986).
[7]D. M. Carey and G. M. Korenowski, J. Chem. Phys. **108**, 2669 (1998).
[8]M. Galvin and D. Zerulla, Chem. Phys. Chem. **12**, 913 (2011).
[9]E. W. Castner, Jr., Y. J. Chang, Y. C. Chu, and G. E. Walrafen, J. Chem. Phys. **102**, 653 (1995).
[10]S. Woutersen and H. J. Bakker, Nature (London) **402**, 507 (1999).
[11]J. B. Asbury, T. Steinal, C. Stromberg, S. A. Corcelli, C. P. Lawrence, J. L. Skinner, and M. D. Fayer, J. Phys. Chem. A **108**, 1107 (2004).
[12]E. T. J. Nibbering and T. Elsaesser, Chem. Rev. **104**, 1887 (2004).
[13]Z. Wang, Y. Pang, and D. D. Dlott, J. Phys. Chem. A **111**, 3196 (2007).
[14]M. L. Cowan, B. D. Bruner, N. Huse, J. R. Dwyer, B. Chugh, E. T. J. Nibbering, T. Elsaesser, and R. J. D. Miller, Nature (London) **434**, 199 (2005).
[15]J. D. Eaves, J. J. Loparo, C. J. Fecko, S. T. Roberts, A. Tokmakoff, and P. L. Geissler, Proc. Natl. Acad. Sci. U.S.A. **102**, 13019 (2005).
[16]J. J. Loparo, S. T. Roberts, and A. Tokmakoff, J. Chem. Phys. **125**, 194521 (2006).
[17]D. Kraemer, M. L. Cowan, A. Paarmann, N. Huse, E. T. J. Nibbering, T. Elsaesser, and R. J. Dwayne Miller, Proc. Natl. Acad. Sci. U.S.A. **105**, 437 (2008).
[18]G. Richmond, Chem. Rev. **102**, 2693 (2002).
[19]Y. R. Shen and V. Ostroverkhov, Chem. Rev. **106**, 1140 (2006).
[20]F. Franks, *Water: A Comprehensive Treatise* (Plenum, New York, 1972), vol. 1.
[21]*Persistent Spectral Hole Burning: Science and Application*, edited by W. E. Moerner (Springer, New York, 1988).
[22]Y. Tanimura and S. Mukamel, J. Chem. Phys. **99**, 9496 (1993).
[23]S. Mukamel, *Principles of Nonlinear Optical Spectrosopy* (Oxford University Press, New York, 1995).
[24]G. R. Fleming and M. Cho, Annu. Rev. Phys. Chem. **47**, 109 (1996).
[25]I. Ohmine and S. Saito, Acc. Chem. Res. **32**, 741 (1999); J. Chem. Phys. **125**, 084506 (2006).
[26]C. P. Lawrence and J. L. Skinner, J. Chem. Phys. **117**, 5827 (2002); **117**, 8847 (2002); **118**, 264 (2003); **119**, 1623 (2003).
[27]B. M. Auer, R. Kumar, J. R. Schmidt, and J. L. Skinner, Proc. Natl. Acad. Sci. U.S.A. **104**, 14215 (2007).
[28]B. M. Auer and J. L. Skinner, J. Chem. Phys. **128**, 224511 (2008); Chem. Phys. Lett. **470**, 13 (2009).
[29]T. Yagasaki and S. Saito, Acc. Chem. Res. **42**, 1250 (2009).
[30]T. Hasegawa and Y. Tanimura, J. Phys. Chem. B **115**, 5545 (2011).
[31]C. J. Tainter, Y. Ni, L. Shi, and J. L. Skinner, J. Phys. Chem. Lett. **4**, 12 (2013).
[32]R. M. Stratt, Acc. Chem. Res. **28**, 201 (1995).
[33]T. Keyes, J. Phys. Chem. A **101**, 2921 (1997).
[34]P. H. Tang, T. M. Wu, T. W. Yen, S. K. Lai, and P. J. Hsu, J. Chem. Phys. **135**, 094302 (2011).
[35]P. H. Tang, T. M. Wu, P. J. Hsu, and S. K. Lai, J. Chem. Phys. **137**, 244304 (2012).
[36]H. L. Li and M. N. Kobrak, Chem. Phys. Chem. **13**, 1934 (2012).
[37]V. I. Clapa, T. Kottos, and F. W. Starr, J. Chem. Phys. **136**, 144504 (2012).
[38]A. J. Green, A. Perry, P. B. Moore, and B. Space, J. Phys. Condens. Matter **24**, 124108 (2012).
[39]M. A. Soler, A. E. Roitberg, T. Nelson, S. Tretiak, and S. Fernandez-Alberti, J. Phys. Chem. A **116**, 9802 (2012).
[40]A. Melzer, A. Schella, J. Schablinski, D. Block, and A. Piel, Phys. Rev. Lett. **108**, 225001 (2012).
[41]R. J. Bell, P. Dean, and D. C. Hibbins-Butler, J. Phys. C **3**, 2111 (1970).
[42]M. Cho, G. R. Fleming, S. Saito, I. Ohmine, and R. M. Stratt, J. Chem. Phys. **100**, 6672 (1994).
[43]F. Sciortino and P. Tartaglia, Phys. Rev. Lett. **78**, 2385 (1997).
[44]S. Saito and I. Ohmine, J. Chem. Phys. **108**, 240 (1998).
[45]H. Ahlborn, X. D. Ji, B. Space, and P. B. Moore, J. Chem. Phys. **111**, 10622 (1999); H. Ahlborn, B. Space, and P. B. Moore, *ibid.* **112**, 8083 (2000).
[46]S. L. Chang, T. M. Wu, and C. Y. Mou, J. Chem. Phys. **121**, 3605 (2004).
[47]K. H. Tsai and T. M. Wu, Chem. Phys. Lett. **417**, 389 (2006).
[48]H. J. C. Berendsen, J. R. Grigera, and T. P. Straatsma, J. Phys. Chem. **91**, 6269 (1987).
[49]K. Toukan and A. Rahman, Phys. Rev. B **31**, 2643 (1985).
[50]J. Marti, J. A. Padro, and E. Guàrdia, J. Mol. Liq. **62**, 17 (1994).
[51]C. P. Lawrence and J. L. Skinner, Chem. Phys. Lett. **372**, 842 (2003).
[52]M. Praprotnik, D. Janežič, and J. Mavri, J. Phys. Chem. A **108**, 11056 (2004).
[53]J. Marti, E. Guàrdia, and J. A. Padro, J. Chem. Phys. **101**, 10883 (1994).
[54]J. Marti, J. A. Padro, and E. Guàrdia, J. Chem. Phys. **105**, 639 (1996).
[55]J. Marti and M. C. Gordillo, Phys. Rev. B **63**, 165430 (2001).
[56]O. Byl, J. C. Liu, Y. Wang, W. L. Yim, J. K. Johnson, and J. T. Yates, Jr., J. Am. Chem. Soc. **128**, 12090 (2006).
[57]N. R. Tummala and A. Striolo, J. Phys. Chem. B **112**, 10675 (2008).
[58]M. E. Parker and D. M. Heyes, J. Chem. Phys. **108**, 9039 (1998).
[59]M. P. Allen and D. J. Tildesley, *Computer Simulation of Liquids* (Clarendon Press, Oxford, 1987).
[60]P. Ewald, Ann. Phys. **369**, 253 (1921).
[61]J. L. Finney, Proc. R. Soc. London, Ser. A **319**, 479 (1970).
[62]G. Ruocco, M. Sampoli, and R. Vallauri, J. Chem. Phys. **96**, 6167 (1992).
[63]R. Ruocco, M. Sampoli, A. Torcini, and R. Vallauri, J. Chem. Phys. **99**, 8095 (1993).
[64]P. Jedlovszky, J. Chem. Phys. **111**, 5975 (1999).
[65]P. Jedlovszky, J. Chem. Phys. **113**, 9113 (2000).
[66]Y. L. Yeh and C. Y. Mou, J. Phys. Chem. B **103**, 3699 (1999).
[67]J. L. F. Abasca, M. A. Gonzalez, J. L. Aragones, and C. Valeriani, J. Chem. Phys. **138**, 084508 (2013).
[68]R. Kumar, J. R. Schmidt, and J. L. Skinner, J. Chem. Phys. **126**, 204107 (2007).
[69]B. M. Auer and J. L. Skinner, J. Chem. Phys. **127**, 104105 (2007).
[70]G. E. Walrafen, Y. C. Chu, and G. J. Piermarini, J. Phys. Chem. **100**, 10363 (1996).
[71]T. M. Wu and R. F. Loring, J. Chem. Phys. **97**, 8568 (1992).
[72]Y. Wan and R. M. Stratt, J. Chem. Phys. **100**, 5123 (1994).
[73]P. Moore and B. Space, J. Chem. Phys. **107**, 5635 (1997).
[74]J. J. Ludlam, S. N. Taraskin, and S. R. Elliott, Phys. Rev. B **67**, 132203 (2003).
[75]B. J. Huang and T. M. Wu, Phys. Rev. E **79**, 041105 (2009).
[76]K. Ohno, M. Okimura, N. Akai, and Y. Katsumoto, Phys. Chem. Chem. Phys. **7**, 3005 (2005).
[77]The average frequency of an INM band is defined as $\omega_X = \int_{\omega_a}^{\omega_b} \omega D_H^{(S)}(\omega)d\omega / I_X$ with $I_X = \int_{\omega_a}^{\omega_b} D_H^{(S)}(\omega)d\omega$, where ω_b and ω_a are the upper and lower limits for the range of the INM band, respectively.
[78]In our calculations, for *Model II*, the range of the bending band is from 1360 cm^{-1} to 1980 cm^{-1} and that of the stretching band is from 2400 cm^{-1} to 5000 cm^{-1}. For *Model I*, the bending band is in a range from 1200 cm^{-1} to 2275 cm^{-1}; the stretching band is from 2275 cm^{-1} to 5000 cm^{-1}.